RAYLEIGH WAVE PARTICLE MOTION AND CRUSTAL STRUCTURE

By David M. Boore and M. Nafi Toksöz

ABSTRACT

A feasibility study was made concerning the use of the ellipticity of the Rayleigh wave particle motion for determining earth structures. Variational parameters were computed empirically for both the ellipticity and phase velocity of Rayleigh waves in the period range $T = 10$–50 seconds. It was found that, in general, the ellipticity and phase velocity are about equally sensitive to structural perturbations, but that near-surface low-velocity sedimentary layers influence the ellipticity much more strongly than they do the phase velocity. Anelasticity has a minor effect on the ellipticity, whereas the presence of interfering waves can have a significant influence.

A test of the independence between ellipticity and phase velocity indicated that in our period range ellipticity does contribute independent information, and thus provides an additional constraint toward uniqueness.

Using data from LASA, both ellipticity and Rayleigh- and Love-wave phase velocities were measured and the results interpreted in terms of a crustal structure. The ellipticity data proved useful when combined with the phase velocity and some structures that fit the phase velocity data could be rejected on the basis of ellipticity.

Introduction

Studies of the phase and group velocity dispersion curves of the Rayleigh and Love waves and their interpretation in terms of layered earth models contributed greatly to our knowledge of the Earth's upper mantle and crustal structure. Another property of the Rayleigh waves that may be useful is the ellipticity of the particle motion at the surface. Unlike the case of an elastic half space, the ellipticity—defined as the ratio of the horizontal to vertical axis of the elliptic trajectory of particle motion—varies with period in the case of layered structures. These variations have been well known theoretically, and in most studies, horizontal and vertical components of the motion have been computed routinely in dispersion calculations. The purpose of this study is to investigate the feasibility of ellipticity measurements from Rayleigh wave seismograms and their interpretation in terms of earth structures.

To test the ellipticity method and to compare it with the phase velocity technique, we need an area where there is crustal structure information and a distribution of stations suitable for phase-velocity measurements. The Large Aperture Seismic Array (LASA) in Montana provides the necessary station density and well-matched three-component instruments. Data from sets of LASA long-period instruments were used in this study for both ellipticity and phase velocity measurements.

In the paper, we will discuss in the next section the theoretical aspects of the ellipticity of Rayleigh-wave particle motion, its dependence on structural parameters and its relationship to phase-velocity data. The analysis and interpretation of the ellipticity- and phase-velocity data will be covered in the third section.

General Considerations

The particle motion of a Rayleigh wave may be thought of as a superposition of particle motions of mono-frequency waves. For such a single-frequency wave propagating over an infinite half space this motion is an ellipse with the vertical and radial

directions as principal axes. This is also true at far-field distances for a wave radiated from an arbitrary point source in a perfectly elastic layered medium (Haskell, 1964), in which case the ratio of the two displacements at the ground surface can be written as

$$\frac{U_H}{U_V} = i \frac{A}{B}$$

where U_H, U_V = spectra of the radial and vertical components of motion, $i = \sqrt{-1}$, and A, B are real functions of frequency and the layer parameters (thicknesses, densities, velocities). This expression holds for any order mode. The ratio is purely imaginary, with an amplitude depending only on frequency and elastic parameters beneath the recording site. Thus a plot of the amplitude of the spectral ratio (which will hereafter be termed "ellipticity") versus frequency can be used in the same manner as a phase velocity dispersion curve for the interpretation of earth structure.

Anelasticity. Haskell (1953) pointed out that the introduction of anelasticity into the problem by the use of complex velocities in A, B would result in a spectral ratio which was no longer purely imaginary, with the consequence that the major axis of the ellipse of particle motion would be inclined with respect to the vertical. This has been observed experimentally (Dobrin *et al*, 1951). One would then hope that measurements of the tilt angle vs. period could be interpreted in terms of the Q-structure of the earth.

To determine the effects of anelasticity we will consider the simplest case of an isotropic half space. The spectral ratio of the surface displacement is given in terms of the velocities $\bar{c}$, $\bar{\alpha}$, $\bar{\beta}$ by:

$$\frac{U_H}{U_V} = - i \frac{(2 - \bar{c}^2/\bar{\beta}^2)}{2\sqrt{1 - \bar{c}^2/\bar{\alpha}^2}} \tag{1}$$

where $\bar{c}$ is the complex phase velocity and $\bar{\alpha}$, $\bar{\beta}$ are the complex compressional and shear velocities in the half space. Following MacDonald (1959) and Press and Healy (1957), anelasticity is introduced by setting

$$\bar{\alpha} = \alpha \left(1 - \frac{i}{2} Q_\alpha^{-1}\right)$$

$$\bar{\beta} = \beta \left(1 - \frac{i}{2} Q_\beta^{-1}\right)$$

$$\bar{c} = c \left(1 - \frac{i}{2} Q_R^{-1}\right)$$

where terms in $(Q_j^{-1})^2$, $j = \alpha$, β, R have been neglected. α, β and c are, for low loss materials, equal to the usual velocities for a perfectly elastic material. Then to first order in Q_j^{-1} we find upon expansion, simplification, and the use of MacDonald's results relating Rayleigh wave absorption, Q_R^{-1}, to the intrinsic absorption Q_β^{-1} and Q_α^{-1}, that

$$\frac{U_H}{U_V} = \frac{-i(2 - b)}{2\sqrt{1 - a}} - \frac{a(2 - b) + m(2b - 2a - ab)}{4(1 - a)\sqrt{1 - a}} \{Q_\beta^{-1} - Q_\alpha^{-1}\} \tag{2}$$

where

$$b \equiv (c/\beta)^2$$

$$a \equiv (c/\alpha)^2$$

$$m = \frac{a(2 - b)(1 - b)}{a(2 - b)(1 - b) - b(1 - a)(2 - 3b)}$$

TABLE 1

STANDARD MODEL FOR PARTIAL DERIVATIVE CALCULATIONS

Layer no.	Thickness (km)	Vp (km/sec)	Vs (km/sec)	ρ (gm/cc)
1	2.7	3.73	2.31	2.35
2	16.4	6.10	3.69	2.85
3	27.5	6.70	3.84	3.00
4	20.0	8.30	4.65	3.49
5	∞	8.30	4.70	3.49
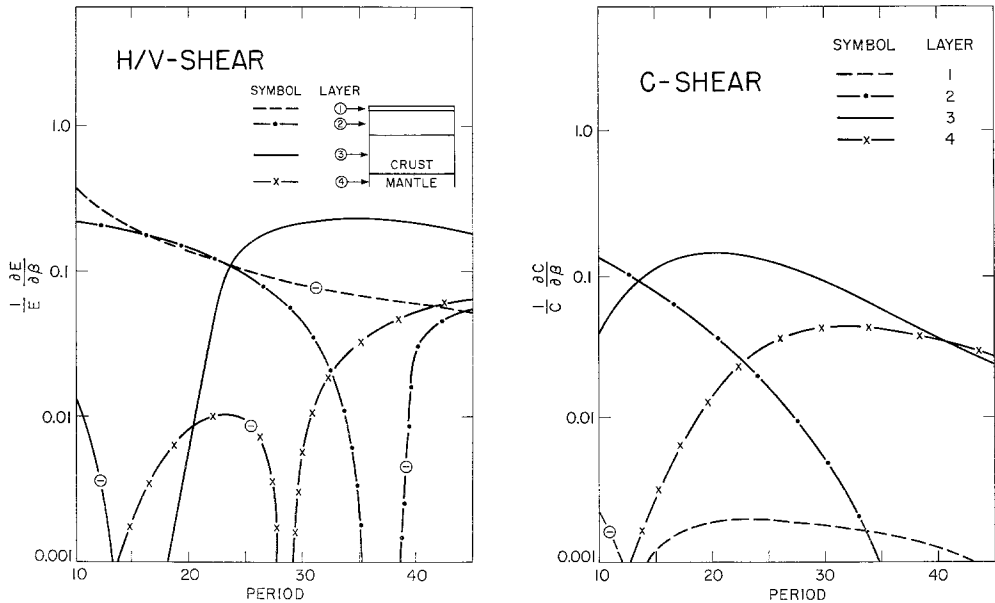
FIG. 1. Normalized partial derivatives of the ellipticity and phase velocity with respect to shear velocity. The circled minus signs indicate negative derivatives.

Thus the spectral ratio when anelasticity is present is equal to that for a perfectly elastic material plus a real term involving the dissipation factors Q_β^{-1}, Q_α^{-1}. The phase introduced in the spectral ratio by this extra term produces a tilt of the particle motion ellipse. For an extreme example let $\beta/\alpha = 0.55$, $Q_\beta^{-1} = 2.5\ Q_\alpha^{-1}$, $Q_\alpha^{-1} = 0.1$. With this data

$$\frac{U_H}{U_V} \cong 0.659 e^{i88°}$$

and the variation from 90° (the phase difference between the horizontal and vertical

components of the motion for an elastic case) is only 2°, a quantity smaller than the experimental scatter. For all practical purposes, therefore, the angle of tilt is negligible and cannot be used to determine the Q-structure, nor does it affect the ellipticity
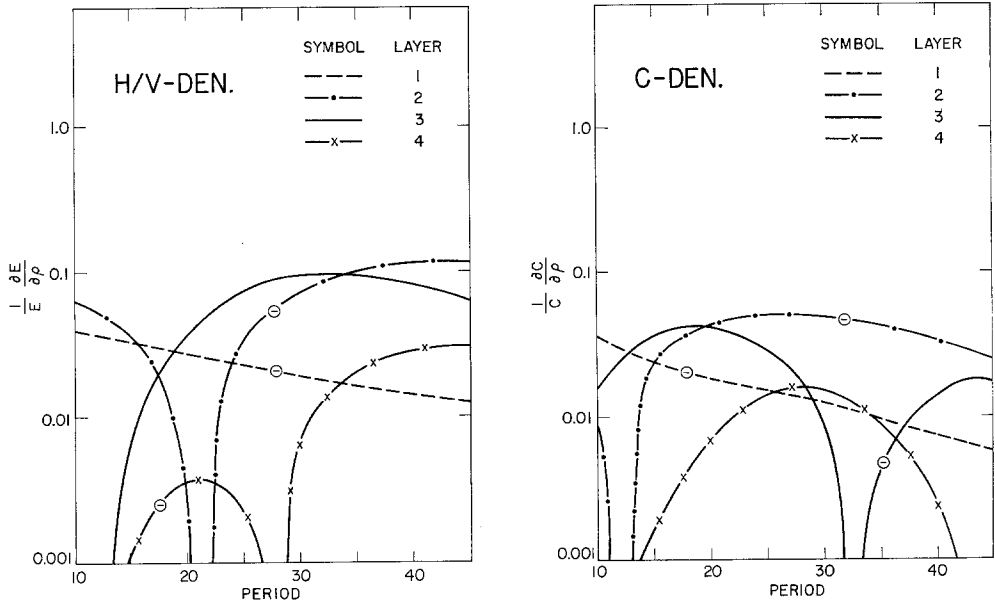
FIG. 2. Normalized partial derivatives of the ellipticity and phase velocity with respect to density.
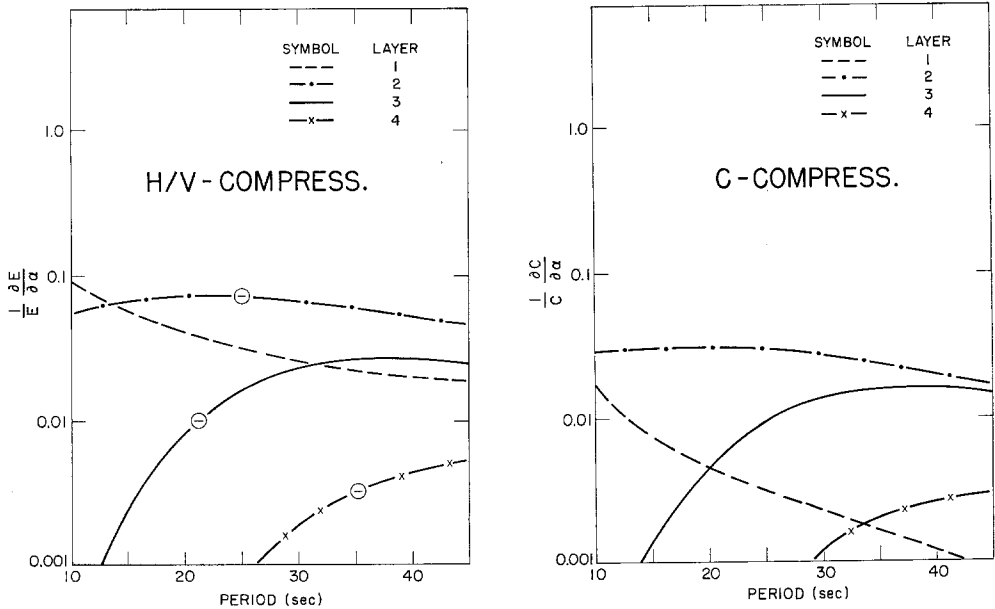
FIG. 3. Normalized partial derivatives of the ellipticity and phase velocity with respect to compressional velocity.

measurements seriously. This result is similar to that obtained, for specific phenomenological models of the attenuation, by Horton (1953) and Nakamura (1957).

Partial derivatives. The usefulness of the technique depends both on the feasibility of making reasonably accurate measurements, and on the sensitivity of the ellipticity

to parameter changes. To study the sensitivity, partial derivative curves were constructed by calculating theoretical ellipticity curves for a suite of models, each of which differs from a standard model (Table 1) by a 10 per cent perturbation of a single layer parameter. For comparison, similar curves were constructed for perturbations of phase velocity. The resulting empirical derivatives, normalized so that a direct comparison between phase velocity and ellipticity is possible, are given in Figures 1, 2, and 3. One conclusion drawn from these figures is that ellipticity is approximately as sensitive to parameter changes as is phase velocity. For a given period, however, the relative location of maxima of corresponding curves indicates that the phase velocity is sensitive to deeper perturbations than is the ellipticity (compressional velocity perturbations seem to be an exception). An important difference between the two sets of curves is the significant dependence, even at long periods, of the ellipticity on the shear velocity in the surficial sedimentary layer (layer 1). This is due to the high sensitivity of the horizontal component of motion to impedance contrasts, such as one gets when low velocity sediments overlie higher velocity basement rocks (Dorman and Prentiss, 1960). This sensitivity may limit the usefulness of the ellipticity method, especially if the structure of the sediments is complicated, for it may cause scatter in the observations and will make an inversion of the data of questionable value. Often, however, the sedimentary structure is known from near surface studies, and if it is uncomplicated (i.e. we can assume that the basement-sediment interface is nearly horizontal in the region of the station) we can eliminate its effect when the inversion is performed. Moreover, the relative flatness of the layer 1 perturbation curves implies that changes in the sedimentary layer will change the ellipticity fairly uniformly at all periods shown in the figures, and thus any "character" in a measured ellipticity curve is probably influenced by other than the near-surface sediments.

The influence of structure within the sediments was determined by breaking layer 1 into three layers and again computing partial derivative curves. The curves effectively differed from one another only by a multiplicative factor, and thus an inversion scheme, such as least-square inversion, using measurements of ellipticity in this period range would not be able to resolve shear velocity differences within the sedimentary layer.

Independence. Since in general the inversion problem is nonunique, that is, there are more unknowns than observables, it is interesting to ask if the addition of the ellipticity measurements to phase velocity measurements will reduce the non-uniqueness by limiting the possible range of valid models. Because of the differing sensitivities of the phase velocity and ellipticity to a given parameter change, as pointed out above, this would seem to be the case. We can get a more quantitative feeling for this by considering the relative independence of certain vectors whose components are partial derivatives. Consider a set of observations of phase velocity (C) and ellipticity (E) at m periods (T). Then

$$E_j = E(T_j) \qquad j = 1, \cdots m$$

$$C_j = C(T_j) \qquad j = 1, \cdots m.$$

If we have an assumed model consisting of n parameters (P) and if this model is close enough to the actual structure, we can linearize and obtain the following equations for the needed perturbations (ΔP) of the assumed model (Dorman and Ewing, 1962)

$$\sum_{i=1}^{n} \frac{\partial C_j}{\partial P_i} \Delta P_i = \Delta C_j \qquad j = 1, 2, \cdots, m \tag{3}$$

$$\sum_{i=1}^{n} \frac{\partial E_j}{\partial P_i} \Delta P_i = \Delta E_j \qquad j = 1, 2, \cdots, m. \tag{4}$$

Each set of equations can be written in matrix form as

$$\begin{bmatrix} \rule{1cm}{0.4pt}V_1\rule{1cm}{0.4pt} \\ \rule{1cm}{0.4pt}V_2\rule{1cm}{0.4pt} \\ \vdots \\ \rule{1cm}{0.4pt}V_m\rule{1cm}{0.4pt} \end{bmatrix} \begin{bmatrix} \Delta P_1 \\ \Delta P_2 \\ \vdots \\ \Delta P_n \end{bmatrix} = \begin{bmatrix} \Delta A_1 \\ \Delta A_2 \\ \vdots \\ \Delta A_m \end{bmatrix}$$

where V_j is a row vector with components

$$V_j = \left(\frac{\partial A_j}{\partial P_1}, \frac{\partial A_j}{\partial P_2}, \cdots, \frac{\partial A_j}{\partial P_n} \right)$$

where $A_j = E_j$ or C_j.

TABLE 2

RESULTS OF ORTHOGONALIZATION

Case I—With near surface layer (Max. no. of indep. vectors in cross set = 15)

TOL	No. indep. C	No. indep. E	No. indep. in cross set
10^{-2}	5	6	10
10^{-3}	7	7	13
10^{-4}	9	9	15

Case II—Without near surface layer (Max. no. of indep. vectors in cross set = 12)

TOL	No. indep.	No. indep. E	No. indep. in cross set
10^{-2}	5	5	9
10^{-3}	6	7	12
10^{-4}	8	9	12

In general, $n > m$ and the system of equations involving just the phase velocity or ellipticity has no unique solution. The question we will consider here is whether the addition of the ellipticity equations (set 4) to the phase velocity equations (set 3) contributes any new information or whether it simply introduces compatibility requirements on the right hand side. That is, are we contributing independent row vectors to the phase velocity row vectors when we include the ellipticity observations? To answer this, vectors were constructed from the calculated partial derivatives and their independence was studied by using a Gram-Schmidt orthogonalization procedure (Fougere, 1963).

In the Gram-Schmidt procedure a set of new orthogonal vectors is systematically constructed from the original set of vectors. If any of the original vectors are linearly dependent, the number of orthogonal vectors will be less than the number of original

vectors; such a linear dependence would theoretically result in the construction of a null vector in the computation scheme. Since in practice we only have a finite number of decimal places in the computations we must introduce a characteristic length, TOL, such that a null vector in the orthogonalization scheme is assumed to be one with length less than TOL. The appropriate TOL depends both on the accuracy of the numerical scheme and the relative accuracy of the vector components and data; in this study a range of values was used.

The results for a standard model with three main crustal layers and a sedimentary
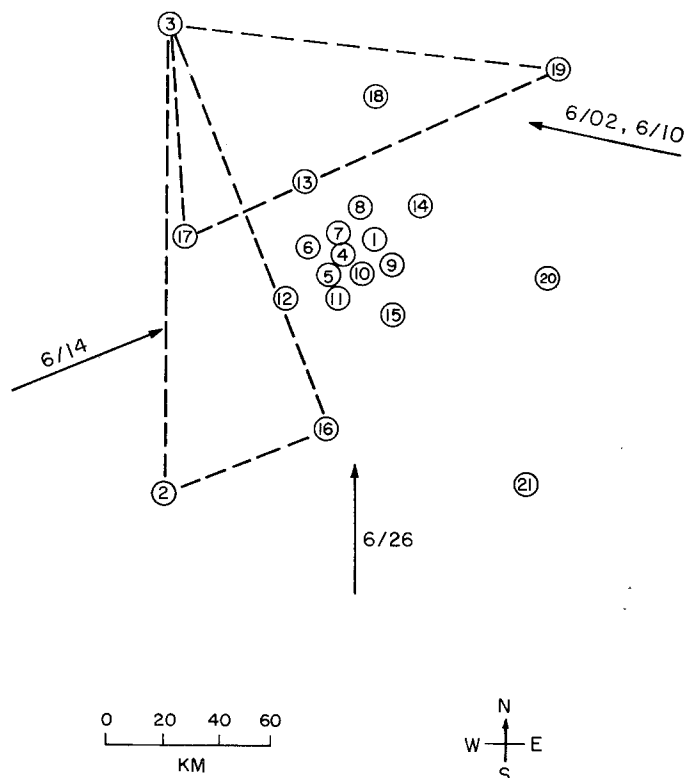
Fig. 4. Plan view of LASA, with the seismometer sites indicated by circled numbers. The various events used in the analysis and their direction of approach are shown by the arrows. The dashed triangles are representative station combinations used in the phase velocity analysis.

layer are given in Table 2. A set of 9 vectors (corresponding to periods $T = 10$ to $T = 50$ seconds), with 15 components in case I and 12 components in case II, were constructed for both ellipticity and phase velocity (i.e., $m = 9$, $n = 15$ and 12 in equations 3 and 4). Case II differs from case I in that variations of parameters in the sediment layer (layer 1) are not considered in case II. Thus out of the 18 vectors in the cross-set (ellipticity row vectors combined with phase velocity row vectors) the maximum number of independent vectors is limited to 15 in case I and 12 in case II. The orthogonalization was first applied separately to the two sets of 9 vectors. For example (Table 2), for case I and TOL $= 10^{-3}$, 6 out of the 9 original phase velocity vectors and 7 out of the 9 original ellipticity vectors were independent. (Although not indicated in the table, the dependent vectors were those constructed for such periods as 40–45–50 seconds. Because the derivative curves flatten out in this range, vectors constructed for such closely spaced periods will be similar and thus,

with the assumed TOL, may be dependent.) A cross-set of the resulting independent vectors in each of the individual sets was then formed and the orthogonalization was again performed. In the example above, 12 of the 13 vectors (6 from the phase velocity set and 7 from the ellipticity set) in the cross-set were found to be independent. This result, and the other results in Table 2, imply that the ellipticity set of equations is nearly independent of the phase velocity set in the period range tested. This is an indication that the ellipticity does contribute independent information, and thus it would be useful to consider both phase velocity and ellipticity together.

EXPERIMENTAL RESULTS

To study the method, ellipticities and phase velocities were measured for several events recorded at LASA in Montana. The site distribution of the array is given in Figure 4 and the epicenter information is listed in Table 3. The data was chosen on the basis of its relative freeness from both noise and complicated amplitude modulation. None of the data, however, was entirely free of modulation effects. Because there are indications (Glover and Alexander, 1968; Greenfield and Shepard, 1968; Fairborn, 1968) that the sub-LASA structure is complicated, only a segment of the northern part of the array was chosen for this study, whose primary purpose was to test the ellipticity method.

TABLE 3
EPICENTER INFORMATION

Date	Origin time	Latitude	Longitude	Magnitude (Mb)	Locality
6/02/67	06.31.28.2	0.9N	28.4W	5.0	Cen. Mid-Atl. Ridge
6/10/67	18.04.39.6	16.4N	46.6W	4.9	N. Atl. Ridge
6/14/67	05.06.16.3	15.2S	173.6W	5.9	Tonga Islands
6/26/67	02.22.34.8	18.4N	105.2W	5.0	Jalisco, Mexico

An equalization for the differing magnifications of the three long-period instruments at a given site was first applied to the data. These magnification factors were found by averaging the magnitudes of approximately 30–40 consecutive peaks and troughs on sine-wave calibration curves recorded on three separate days. Differences in magnification between the components at a given site were on the order of 5 per cent. Unfortunately, the calibration tests at LASA are restricted to a single frequency, thus necessitating the assumption that the equalization factors are independent of frequency.

After equalization the horizontal components were rotated into radial and transverse directions, using azimuths derived from preliminary time-domain phase velocity studies. For simplicity frequency-independent azimuths were assumed. If no Love waves are present, the error in the horizontal spectrum due to misrotation is second order in the azimuthal error, and is thus usually small. Fourier transforms of the vertical and rotated traces were calculated and a moving, equal-weight average of seven adjacent points was used to smooth the amplitude spectra before the ellipticity was computed. This averaging seemed to have the desired effect of smoothing the ellipticity without introducing any noticeable bias.

Examination of the measured ellipticity revealed two features which could not be explained by homogeneous, isotropic plane-layered structures: (1) relative peaks and troughs occurring within narrow period ranges which are associated with nulls in the

amplitude spectra; (2) a suggestion of a separation of curves corresponding to events coming from different azimuths. The second observation is, because of the small number of events studied and the scatter of the measured data, only tentative and may be explained by the presence of anisotropy or non-planar, laterally inhomogeneous structures. The first observation is more amenable to measurement and analysis. A particularly clear example of the phenomena is shown in Figure 5, with the amplitude spectra and corresponding seismograms from which the ellipticity was computed given in Figure 6. The obvious beat in the seismogram and the peak in the ellipticity are both associated with the pronounced null in the amplitude spectra at 20.88 sec. Pilant and Knopoff (1964) showed that such amplitude modulation in the time domain and minima in the amplitude spectrum can be considered an interference effect. (In this case the null in the spectrum is definitely not a source effect, since relatively little interference is observed at some other sites in the array). By modeling this interference as an interaction of two dispersive waves impinging at an angle to
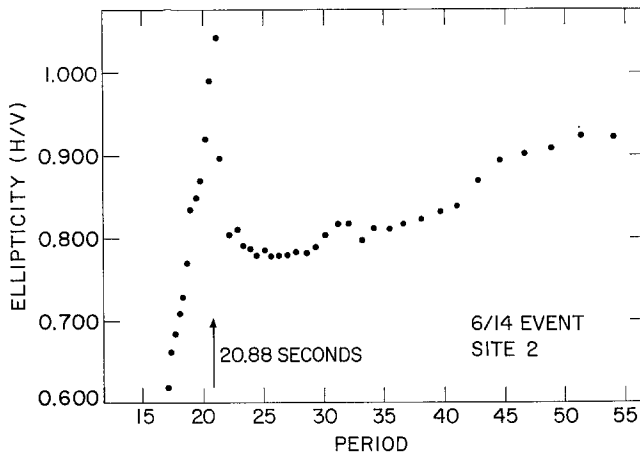
FIG. 5. Measured ellipticity, showing the effects of interference.

one another and with a relative time lag between them (see the Appendix), one finds that relative peaks should occur in the ellipticity at the null-periods of the amplitude spectra. Thus we can argue that such peaks, if correlated with minima in the amplitude spectrum, are not due to elastic structure and we can eliminate them if the interference parameters can be estimated.

Even after accounting for the interference, considerable scatter remained in the data. The magnitude of this scatter was such that it was not considered worthwhile to derive crustal models from the ellipticity measured at separate sites. Rather, an average of the ellipticity from several sites was used in conjunction with phase velocity to derive an earth model. The ellipticity data is given in Figure 7, along with a theoretical curve for a derived model. The ellipticity values were taken from all the events measured excluding that on 6/26, and include data from the following sites: 3, 7, 10, 11, 13, 18, 19 (see Figure 4 for the site locations). The amount of data included for a particular event at a particular site depended on the magnitude of the amplitude spectra, contamination from interference, and closeness of the phase-difference between the radial and vertical traces to $-90°$. The phase difference of the retained data was usually with $\pm10°$ of $-90°$. For some events data from a particular site was not included because it showed poor consistency with data from nearby sites.

For example, for the 6/14 event, sites 7, 10, and 11 gave remarkably consistent ellipticity, but the data from site 5 was very different. The cause of this difference is not known. The data near interference peaks (usually between 20 and 30 seconds) was also not included. Because of the difficulty of estimating the interference parameters, no corrections were applied to the data remaining after this elimination. Qualitatively, the corrections would move the ellipticity points for periods greater than 30 seconds closer to the theoretical curve.

Phase velocities of the Rayleigh and Love waves from various events were also computed using various combinations of stations. It was possible, as indicated in Figure 4, to find combinations of 3 sites such that the propagation vector of an event
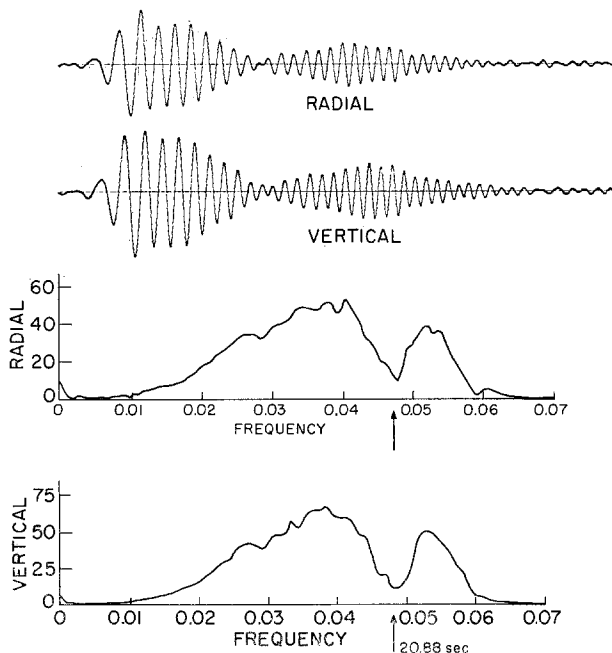
FIG. 6. Time series and corresponding amplitude spectra used in the calculation of the ellipticity in Figure 5.

was almost parallel with the long leg of the resulting triangle. Measurements of the phase velocity for different triangles in the northern part of the array gave similar dispersion, but results from the south-half of the array were different, indicating a lateral variation between the two parts. The results for the northern part only are included in this paper (Figure 8). As for the ellipticity, data from the different events, measured over different combinations of sites, were included in the figure. Measurements were done in the frequency domain using standard phase difference techniques (Toksoz and Ben-Menahem, 1963). A redundancy in the measurements was possible since a given triangle contained more than three stations, and thus the results obtained are least-square determinations of phase velocity. Different types of phase smoothing, using linear and quadratic running averages, were tried. Results from such smoothing operations are included in Figure 8 only if the unsmoothed phase velocities did not exhibit large oscillations (presumably an interference phenomena) or scatter. Due to the lack of calibration data, no corrections for instrument response were applied. The instruments are well-matched, however, and such corrections are expected to be small.

Interpretation. A model (M1) which fits both Rayleigh wave phase velocity and ellipticity fairly well is given in Table 4. This model was found by using a combination of trial-and-error and least-square numerical inversion techniques. The apparent discrepancy between the theoretical and observed Love wave dispersion is not to be taken seriously at the present, for the Love wave data are based on only one event
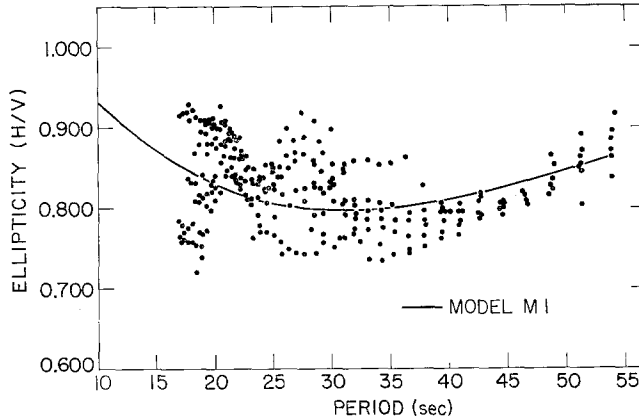
Fig. 7. Measured ellipticity for different events and different sites. The solid line is the theoretical ellipticity corresponding to model M1.

TABLE 4

EARTH MODELS

M1—Derived LASA model

Thickness (km)	Vp(km/sec)	Vs(km/sec)	ρ(gm/cc)
1.75	3.60	2.16	2.50
17.50	6.15	3.71	2.90
17.00	6.97	3.92	3.10
16.00	7.20	3.92	3.15
∞	8.20	4.75	3.65

M2—Comparison model

Thickness (km)	Vp(km/sec)	Vs(km/sec)	ρ(gm/cc)
2.8	3.55	2.10	2.51
17.5	6.08	3.61	2.85
17.0	6.97	4.06	3.10
16.5	7.85	4.36	3.22
∞	8.07	4.65	3.55

and are considered preliminary. Further measurements are in progress. A starting point for the inversion was given by the seismic refraction surveys (Borcherdt and Roller, 1967; Steinhart and Meyer, 1961) and near-surface studies (summarized by Brown and Poort, 1965) in the area. Both refraction surveys indicate a crustal thickness of 47–52 km and a compressional velocity near 6.1 km/sec in the first major crustal layer. The results presented by Steinhart and Meyer differ from those of Borcherdt and Roller in that the former indicate a lower Pn velocity, and higher compressional velocities in the lower half of the crust. The compressional velocities in model M1 are a compromise between the two surveys. The derived shear velocity

structure, however, indicates that the crust can be divided into two main layers in the northern region of LASA and thus supports the Borcherdt and Roller refraction model. Because of the sensitivity of phase velocity and ellipticity to shear velocity, we feel that the distribution with depth of this parameter is a good approximation to the actual structure. An observed flattening of the Rayleigh wave phase-velocity curve for periods greater than 45 seconds (not completely shown in Figure 8) indicates that
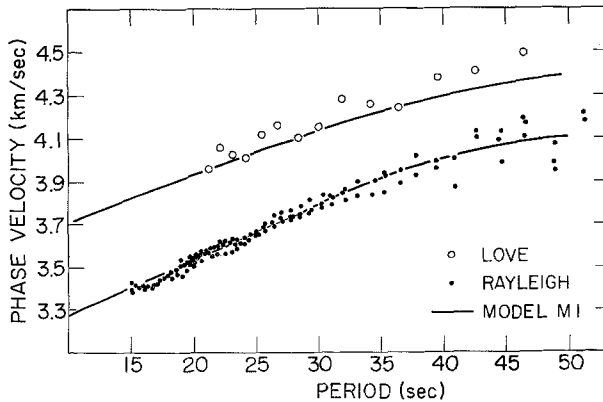
FIG. 8. Measured phase velocities for different events. Only one event, on 6/26/67, was used in the Love wave dispersion measurements.
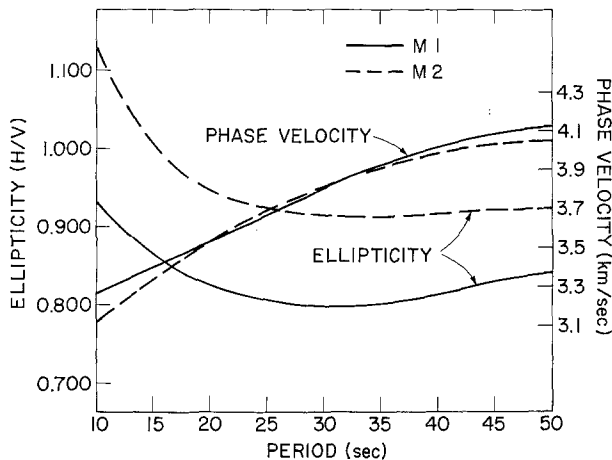
FIG. 9. Theoretical ellipticity and phase velocity for two models, showing the possible use of ellipticity as a discriminant between the models.

a low velocity zone may exist under LASA, but because of the unavailability of ellipticity data at periods long enough to be influenced by this structure such a zone was not included in the interpretation. Because there is an inherent nonuniqueness in the interpretation which cannot be resolved with the quality and period range of data available, and since we are assuming a homogeneous, plane-layered structure, the details of model M1 should not be considered exact.

In the interpretation process the phase velocity, because it exhibited much less scatter, was weighted more heavily than the ellipticity. The ellipticity, however, proved to be a useful constraint in the interpretation. By using it, several parameters

were changed and several models which fit the phase velocities were eliminated. As an illustration of the latter, Figure 9 contains the theoretical curves for two different models, M1 and M2 (Table 4). In the period range at which data is available it is difficult to distinguish between the two models on the basis of the phase velocity alone, but by using the ellipticity data, model M2 is easily eliminated. Of course, the relative separation between the curves must be considered in terms of the accuracy of the data.

Conclusions

The ellipticity of the Rayleigh wave particle motion measured at the Earth's surface as a function of frequency can be an effective tool to study internal structure. Its disadvantages are that it is sensitive to low-velocity near-surface sediments, and that it is difficult to measure with the precision needed to use it alone in the interpretation of earth structure. It has the advantage, however, that it requires data only at one recording site. Also, in the period range of this study (10–50 seconds) ellipticity provides information independent from phase-velocity data. Thus, the combination of the ellipticity and phase-velocity dispersion data should reduce the nonuniqueness in the inversion process.

Measurements of ellipticity using LASA data were of sufficient accuracy to justify their use in combination with the more accurate phase-velocity data in an interpretation of the crustal structure beneath part of the array. A crustal model was found that agreed with both sets of data and also with previous geophysical studies made in the area. In deriving this model the ellipticity data proved to be a useful constraint, for it was possible to eliminate several models which fit the phase velocity data but not the ellipticity.

Appendix

Interference Calculations

Consider the interaction of two Rayleigh waves, with horizontal displacements $h_1(\mathbf{r}, t)$, $h_2(\mathbf{r}, t)$, where the angle between the displacements is $\Delta\phi$ and $\mathbf{r}$ is the position vector of the point $P(x, y)$. Assume that no Love wave energy is present. By rotating the orthogonal horizontal outputs of a seismograph at the point $P(x, y)$ into the $h_1(\mathbf{r}, t)$ direction we obtain the following "radial" time series

$$h(\mathbf{r}, t) = h_1(\mathbf{r}, t) + \cos(\Delta\phi) h_2(\mathbf{r}, t). \tag{1A}$$

If we assume that the structure beneath the station is horizontally plane-layered, we can write

$$h_j(\mathbf{r}, t) = \frac{1}{2\pi} \int_{-\infty}^{\infty} S(\omega) V_j(\omega) e^{i(\omega t - \mathbf{k}_j \cdot \mathbf{r})} \, d\omega \qquad j = 1, 2 \tag{2A}$$

where

$$V_j(\omega) = \int_{-\infty}^{\infty} v_j(0, t) e^{-i\omega t} \, dt \qquad j = 1, 2$$

and v_1, v_2 are the vertical displacements at the origin ($\mathbf{r} = 0$), $\mathbf{k}_j(\omega)$ is the wave number vector, $i = \sqrt{-1}$, and $S(\omega)$ is the actual ellipticity.

We now assume that at the origin

$$V_2(\omega) \;=\; \gamma V_1(\omega) e^{-i\omega\tau(\omega)} \tag{3A}$$

that is, $V_2(\omega)$ differs from $V_1(\omega)$ by a constant scale factor and a frequency dependent time lag. This form of $V_2(\omega)$ is general enough for our purposes and is probably a good approximation to what is physically taking place in interference phenomena.

By substituting (3A) and (2A) into (1A) we can write the measured radial spectrum as

$$H(\mathbf{r}, \omega) \;=\; S(\omega)V_1(\omega)e^{-i\omega x/c}\{1 \,+\, \gamma \cos \Delta\phi e^{-i\omega\tau'(\omega)}\} \tag{4A}$$
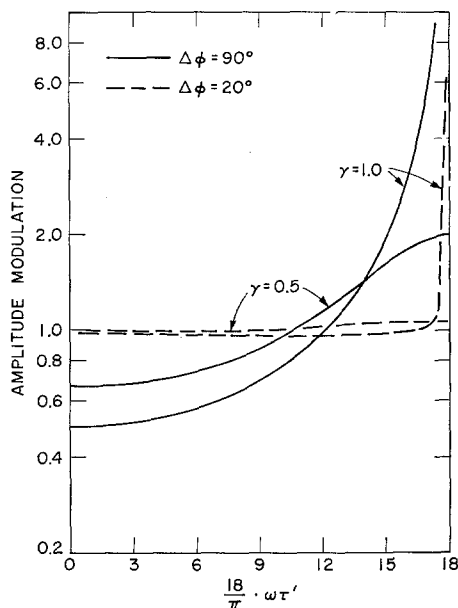
FIG. 10. Amplitude modulation due to interference; equals 1 when no modulation is present.

and by a similar substitution the observed vertical spectrum as

$$V(\mathbf{r}, \omega) \;=\; V_1(\omega)e^{-i\omega x/c}\{1 \,+\, \gamma e^{-i\omega\tau'(\omega)}\} \tag{5A}$$

where $\tau'(\omega) \;=\; \tau \,+\, 1/c\{x \cos \Delta\phi \,+\, y \sin \Delta\phi\} \,-\, x/c$. Here we have assumed an $x - y$ coordinate system with $\mathbf{k}_1$ in the x-direction. Then the measured spectral ratio $H(\mathbf{r}, \omega)/V(\mathbf{r}, \omega)$ can be related to the actual ratio $S(\omega)$ by

$$\frac{H(\mathbf{r}, \omega)}{V(\mathbf{r}, \omega)} \;=\; S(\omega) \cdot \text{AMP} \; e^{i\text{PHASE}} \tag{6A}$$

where AMP and PHASE are modulation factors depending both on frequency and spatial position. They are given by

$$\text{AMP} \;=\; \left[\frac{1 \,+\, 2\gamma \cos \Delta\phi \cos \omega\tau' \,+\, \gamma^2 \cos^2 \Delta\phi}{1 \,+\, 2\gamma \cos \omega\tau' \,+\, \gamma^2} \right]^{1/2} \tag{7A}$$

$$\text{PHASE} = -\tan^{-1} \frac{\gamma \cos \Delta\phi \sin \omega\tau'}{1 + \gamma \cos \Delta\phi \cos \omega\tau'} + \tan^{-1} \frac{\gamma \sin \omega\tau'}{1 + \gamma \cos \omega\tau'} \qquad (8A)$$

where τ' was given earlier. Values of these factors were computed for a wide range of $\omega\tau'$, γ, and $\Delta\phi$. Representative curves are plotted in Figures 10 and 11. As long as $\Delta\phi \leq 90°$, a minimum in the $H(\mathbf{r}, \omega)$ and $V(\mathbf{r}, \omega)$ spectra is always accompanied by a peak in AMP, and thus a peak in the computed ellipticity AMP $\times |S(\omega)|$.

ACKNOWLEDGMENTS
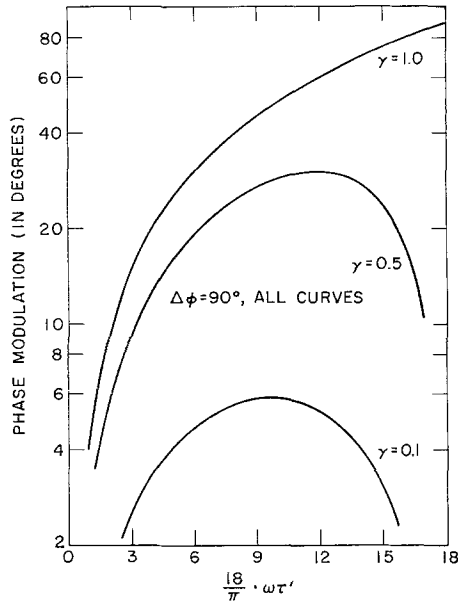
FIG. 11. Phase modulation caused by interference.

REFERENCES

Borcherdt, C. A. and J. C. Roller (1967). Preliminary interpretation of a seismic-refraction profile across the Large Aperture Seismic Array, Montana, *USGS Tech-Letter No. NCER-2*, U. S. Geological Survey, Menlo Park.

Brown, T. G. and J. M. Poort (1965). Subsurface studies and shallow-hole preparation–LASA area, eastern Montana, *Tech. Rep. No. 65-21*, Geotechnical Corp., Garland.

Dobrin, M. B., R. F. Simon and P. L. Lawrence (1951). Rayleigh waves from small explosions, *Trans. Am. Geophys. Union* **32**, 822–832.

Dorman, J. and M. Ewing (1962). Numerical inversion of seismic surface wave dispersion data and crust-mantle structure in the New York-Pennsylvania area, *J. Geophys. Res.* **67**, 5227–5241.

Dorman, J. and D. Prentiss (1960). Particle amplitude profiles for Rayleigh waves on a heterogeneous earth, *J. Geophys. Res.* **65**, 3805–3816.

Fairborn, J. (1968). *P*- and *S*-wave mantle velocities determined from dT/dΔ measurements, *Ph.D. thesis*, Dept. of Geology and Geophysics, Mass. Inst. of Technology.

Fougere, P. F. (1963). Spherical harmonic analysis—1. A new method and its verification, *J. Geophys. Res.* **68**, 1131–1139.

Glover, P. and S. Alexander (1968). Lateral variations in crustal structure beneath the Montana LASA, *Seismic Data Lab. Rep. No. 205*, Teledyne, Alexandria.

Greenfield, R. and R. Shepard (1968). The Moho depth variations under the LASA and their effects on dT/dΔ measurements, to be published in *Bull. Seism. Soc. Am.* **58**.

Haskell, N. A. (1953). The dispersion of surface waves in multilayered media, *Bull. Seism. Soc. Am.* **43**, 17–34.

Haskell, N. A. (1964). Radiation pattern of surface waves from point sources in a multilayered medium, *Bull. Seism. Soc. Am.* **54**, 377–393.

Horton, C. W. (1953). On the propagation of Rayleigh waves on the surface of a visco-elastic solid, *Geophysics* **18**, 70–74.

MacDonald, J. R. (1959). Rayleigh-wave dissipation functions in low-loss media, *Geophys. J.* **2**, 132–135.

Nakamura, K. (1957). On Rayleigh waves propagated over the surface of a medium with elastic after working, *Tōhoku Univ. Sci. Repts. Ser. V*, **9**, 36–44.

Pilant, W. L. and L. Knopoff (1964). Observations of multiple seismic events, *Bull. Seism. Soc Am.* **54**, 19–39.

Press, F. and J. Healy (1957). Absorption of Rayleigh waves in low-loss media, *Jr. Appl. Phys.* **28**, 1323–1325.

Steinhart, J. S. and R. P. Meyer (1961). *Explosion studies of continental structure*, Publ. 622, Carnegie Inst. Washington.

Toksöz, M. N. and A. Ben Menahem (1963). Velocities of mantle Love and Rayleigh waves over multiple paths, *Bull. Seism. Soc. Am.* **53**, 741–764.

DEPARTMENT OF GEOLOGY AND GEOPHYSICS
MASSACHUSETTS INSTITUTE OF TECHNOLOGY
CAMBRIDGE, MASSACHUSETTS 02139